Multi-scale fibre-based optical frequency combs: science, technology and applications (MEFISTA)

Deliverables D1.5 Passive PM fibre ring cavity including a PM FBG

Project details

Project Number	861152	Project Acronym	MEFISTA
Project Title	Multi-scale fibre-based optical frequency combs: science, technology and applications		
Project website	https://mefista.astonphotonics.uk/		
Starting date	01/02/2020		
Project duration	48		
Call (part) identifier	H2020-MSCA-ITN-2019		
Topic	MSCA-ITN-2019 Innovative Training Network		

Document details

Title	Passive PM fibre ring cavity including a PM FBG		
Deliverable number	D5	Deliverable Rel. number	D1.5
Work Package	WP1		
Deliverable type	Report		
Description	Passive PM fibre ring cavity including a PM FBG		
Deliverable due date	31st January 2022		
Actual date of submission	13th February 2023		
Lead beneficiary	ULille		
Version number	V1.0		
Status	Final, public		

Dissemination level

Public (PU)	X
Confidential, only for members of the consortium (including Commission Services)	

Contents

The model: 3
Lugiato-Lefever Equation model: 5
Steady State and Stability Analysis of the LLE model 6
Examples of Gain and integration of LLE 7
Conclusion: 12
Next steps: 12
References: 12

Passive PM fibre ring cavity including a PM FBG

A fiber cavity is, in general, a piece of fiber close in a circle in which the light is able to coherently interact with itself, and produce a wide range of different phenomena. Our focus is study what is the apport of the use of a filter, in our case a fiber Bragg grating, inside the cavity as mean of stimulating modulation instability.
The phenomenon of GTF is well described in some articles, see [1] and [2], but it's analysed for standard fibers. In this preliminary study we explore the effect of using a polarization maintaining fiber and FBG, with the aim of stimulating double frequency. Double frequency combs have different kind of application, from spectroscopy to Lidars, and are characterized by two different but coherent frequency combs, with a small difference in their repetition rate.

The model:

The problem of PM cavity and FBG can be described by a vectorial Ikeda map approach, in which the propagation of the two orthogonally linearly polarized field $A_{x,y}$ is described by a system o two coupled nonlinear Schrödinger equations:

$$\frac{\partial A_x}{\partial z} = \Delta\beta_1 \frac{\partial A_x}{\partial t} - i\frac{\beta_2}{2}\frac{\partial^2 A_x}{\partial t^2} + i\gamma\left(|A_x|^2 + \sigma|A_y|^2\right)A_x = 0\,, \qquad (1)$$

$$\frac{\partial A_y}{\partial z} = -\Delta\beta_1 \frac{\partial A_y}{\partial t} - i\frac{\beta_2}{2}\frac{\partial^2 A_y}{\partial t^2} + i\gamma(|A_y|^2 + \sigma|A_x|^2)A_y = 0.$$

Being at the same frequency we assume that both polarizations have the same group velocity dispersion β_2 and Kerr nonlinearity γ. The group velocity mismatch is defined as $\Delta\beta_1 = \frac{\beta_{1x}-\beta_{1y}}{2}$, where $\beta_{1x,1y}$ is the first derivative of the propagation constant $\beta(\omega)$ respect to ω, $\sigma = \frac{2}{3}$ describes the strength of the cross-polarization interaction. This system describes the evolution of the fields for $0 < z < L$, where L is the total length of the cavity.
When $z = L$ the boundary conditions, Eqs. (2) and (3), include the effects of injection, linear cavity detuning, coupler losses and the filter.

$$A_x^{n+1}(z=0,t) = \theta E_x + \rho e^{i\Phi_{0x}} A_x^n(z=L,t) \star h(t), \qquad (2)$$

$$A_y^{n+1}(z=0,t) = \theta E_y + \rho e^{i\Phi_{0y}} A_y^n(z=L,t) \star h(t), \qquad (3)$$

Where $E_x = E_{IN}\cos(\chi)$, $E_y = E_{in}sin(\chi)$, E_{IN} is the amplitude of the injection and χ characterise the orientation of the injection. The coupler has a reflectivity of ρ and a transmittance of θ. For simplicity the losses are lumped into ρ, so that $1-\rho^2$ accounts for the overall power losses in a roundtrip. $\phi_{0x,y} = \beta(\omega_p)L\ (mod\ 2\pi)$ is the linear phase shift per roundtrip modulo $2\,\pi$. $h(t)$ is the

impulsive response of the filter, and ⋆ represent the convolution operation. We can rewrite the boundary condition in the frequency domain through Fourier transformation:

$$\hat{A}_x^{n+1}(z=0,\omega) = \theta E_x \delta(\omega) + \rho e^{i\phi_{0x}} \hat{A}_x^n(z=L,\omega)H(\omega), \qquad (2)$$

$$\hat{A}_y^{n+1}(z=0,\omega) = \theta E_y \delta(\omega) + \rho e^{i\phi_{0y}} \hat{A}_y^n(z=L,\omega)H(\omega), \qquad (3)$$

Where $\delta(\omega)$ is the Dirac delta function and $H(\omega)$ is the transfer function of the filter.

In general, the filter is described through the following model [2]:

$$H(\omega) = e^{F(\omega)+i\psi(\omega)}, \qquad (4)$$

$$F(\omega) = b\frac{a^4}{(\omega-\omega_f)^4 + a^4}, \qquad (5)$$

$$\psi(\omega) = ba\frac{(\omega-\omega_f)[(\omega-\omega_f)^2 + a^2]}{\sqrt{2}\,[(\omega-\omega^4) + a^4]}, \qquad (6).$$

Equations (5) and (6) describes the loss profile and the phase of the filter respectively, the parameter a is related to the filter bandwidth (rad/s), while the parameter b is a non dimensional number which controls the maximum attenuation of the filter.
Since the filter considered in this study is engraved into a PM cavity, the model has to account for the effect of the birefringence. The two axes of propagation of a PM fiber have two different refractive indexes, which brings to two different Bragg wavelength of the filters: $\lambda_s = 2\,\Lambda\,\mathrm{n}_{eff}^{\mathrm{s}}$ and $\lambda_f = 2\,\Lambda\,\mathrm{n}_{eff}^{\mathrm{f}}$, where Λ is the grating period, $\lambda_{s,f}$ and $\mathrm{n}_{eff}^{\mathrm{s,f}}$ are the Bragg wavelength and effective refractive indexes of the slow and fast axis, respectively.
An example of PM filter modelled with eq (4) is reported in Fig.(1). In the plot we divided the transfer function and phase of the fast and slow axis, calculated according to eqs. (5) and (6).

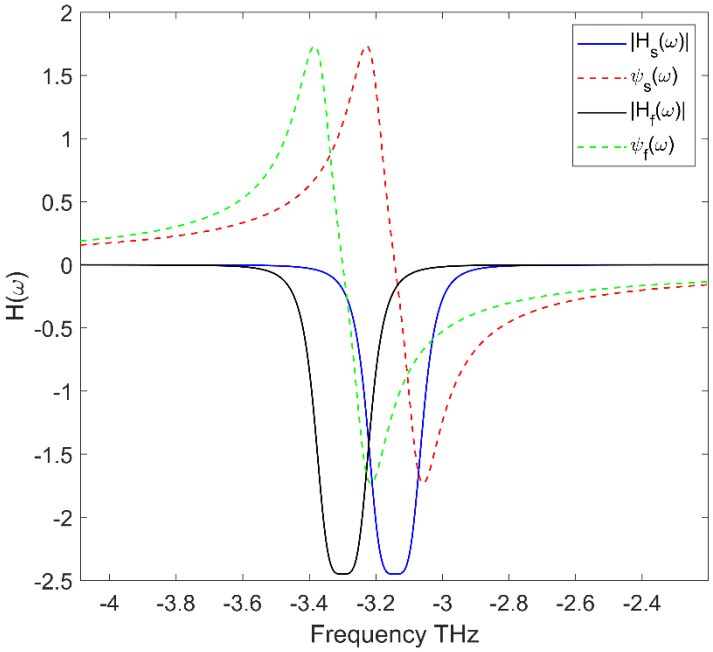

Fig. 1: Typical response of the filter with the model described by Eqs. (5) and (6). $a = 85e^{9} rad/s$, $b = -2.45$, $w_s = -314\ GHz$, $w_f = -329\ GHz$, respect to the pump frequency.

Lugiato-Lefever Equation model:

Starting from the coupled system of Eqs. (1),(2) and (3), it's possible to derive the respective LLE model, which reduce in a system of two coupled equations.
The derivation is done under the good cavity approximation ($\rho \approx 1, \theta \ll 1$), and assume that the intracavity field doesn't change drastically from round-trip to round-trip.
By performing a suitable averaging of Ikeda map, it's possible to obtain the following system of coupled equations:

$$L\frac{\partial A_x}{\partial z} = [-\alpha + i\,\phi_{0x} + \Phi_x \star + i\,\Psi_x \star]A_x + \left[+ L\,\Delta\beta_1 \frac{\partial}{\partial t} - \frac{iL\beta_2}{2}\frac{\partial^2}{\partial t^2} + i\,L\,\gamma(|A_x|^2 + \sigma|A_y|^2)\right]A_x + \theta E_x\,, \qquad (7)$$

$$L\frac{\partial A_y}{\partial z} = [-\alpha + i\,\phi_{0y} + \Phi_y \star + i\,\Psi_y \star]A_y + \left[- L\,\Delta\beta_1 \frac{\partial}{\partial t} - \frac{iL\beta_2}{2}\frac{\partial^2}{\partial t^2} + i\,L\,\gamma(|A_y|^2 + \sigma|A_x|^2)\right]A_y + \theta E_y, \qquad (8)$$

Where $\Phi_{x,y}$ and $\Psi_{x,y}$ being the Fourier anti-transform of Eqs. (8) and (9) referred to the appropriate axes of propagation. We consider the linear losses α as equal on both axes, as well as the coupler description (ρ, θ).

Steady State and Stability Analysis of the LLE model

By looking for the homogeneous state of the field inside the cavity ($\frac{\partial}{\partial z} = \frac{\partial}{\partial t} = 0$), it's possible to find the relation between the intracavity power and the input power as:

$$\bar{P}_x = \frac{\theta^2}{\left(-\alpha + F_x(0)\right)^2 + (\phi_{0x} + \psi_x(0) + \gamma L\, \bar{P}_x)^2} P_{INx}, \quad (9)$$

$$\bar{P}_y = \frac{\theta^2}{\left(-\alpha + F_y(0)\right)^2 + \left(\phi_{0y} + \psi_y(0) + \gamma L\, \bar{P}_y\right)^2} P_{INy}. \quad (10)$$

Where $P_{INx,y} = \left|E_{x,y}\right|^2$.

We then perform a linear stability analysis on the homogeneous solution by inserting the ansatz:

$$A_x(z,t) = A_{0x} + A_x^+(z)e^{-i\omega t} + A_x^- e^{+i\omega t}, \quad (11)$$

$$A_y(z,t) = A_{0y} + A_y^+(z)e^{-i\omega t} + A_y^- e^{+i\omega t}, \quad (12)$$

With $A_{ox} = \sqrt{\bar{P}_x}e^{-i\zeta}$ and $A_{ox} = \sqrt{\bar{P}_y}$, being ζ a phase factor and $A_{x,y}^{\pm}$ the amplitudes of perturbations oscillating at $\mp\omega$ respect to the CW homogeneous solutions, on the respective x and y axes. By linearizing the system of Eqs. (7) and (8), it's possible to compute the propagation matrix M, system (13), which describes the evolution in space of the perturbations $A_{x,y}^{\pm}(z,\omega)$. In the description below, we omit the dependencies from space and frequency of the perturbations and, to get a more readable formulation, we define the diagonals (m_{dk}) and non diagonals (m_k) elements of M separately.

$$\frac{\partial}{\partial z}\begin{bmatrix} A_x^+ \\ A_x^- \\ A_y^+ \\ A_y^- \end{bmatrix} = M \begin{bmatrix} A_x^+ \\ A_x^- \\ A_y^+ \\ A_y^- \end{bmatrix}, (13)$$

$$M = \begin{bmatrix} m_{d1} & m_2 & m_3 & m_3 \\ -m_2 & m_{d2} & -m_3 & -m_3 \\ m_3 & m_3 & m_{d3} & m_4 \\ -m_3 & -m_3 & -m_4 & m_{d4} \end{bmatrix}$$

$$C_x = (-\alpha + i\phi_{0x} + F_x(\omega) + \psi(\omega))/L$$

$$C_{x1} = (-\alpha + i\phi_{0x} + F_x(-\omega) + \psi(-\omega))/L$$

$$C_y = (-\alpha + i\phi_{0y} + F_y(\omega) + \psi_y(\omega))/L$$
$$C_{y1} = (-\alpha + i\phi_{0y} + F_y(-\omega) + \psi_y(-\omega))/L$$

$$m_{d1} = C_x + i\,\Delta\,\beta_1\,\omega + i\frac{\beta_2}{2}\omega^2 + i\,\gamma\left(2\,\bar{P}_x + \sigma\bar{P}_y\right)$$
$$m_{d2} = C_{x_1} + i\,\Delta\,\beta_1\,\omega - i\frac{\beta_2}{2}\omega^2 - i\,\gamma\left(2\,\bar{P}_x + \sigma\bar{P}_y\right)$$
$$m_{d3} = C_y - i\,\Delta\,\beta_1\,\omega + i\frac{\beta_2}{2}\omega^2 + i\,\gamma\left(2\,\bar{P}_y + \sigma\bar{P}_x\right)$$
$$m_{d4} = C_{y1} - i\,\Delta\,\beta_1\,\omega - i\frac{\beta_2}{2}\omega^2 - i\,\gamma\left(2\,\bar{P}_y + \sigma\bar{P}_x\right)$$

$$m_2 = i\,\gamma\bar{P}_x$$
$$m_3 = i\,\gamma\,\sigma\sqrt{(\bar{P}_x\bar{P}_y)}$$
$$m_4 = +i\,\gamma\bar{P}_y$$

Given the complexity of the problem, we weren't able to compute a compact formulation for the gain. To compute it we had to follow a numerical procedure: for each ω we diagonalized the M. From the diagonalization we get four eigenvalues $\lambda_{1,2,3,4}(\omega)$, that can be use to compute the gain as $g_{LLE}(\omega) = 2\max[Real(\lambda_{1,2,3,4}(\omega))]$.
It follows that the power of the perturbations $|A^{\pm}_{x,y}|^2$ grows exponentially as $\exp(g_{LLE}(\omega)z)$ when $g_{LLE}(\omega) > 0$.

Examples of Gain and integration of LLE

In this section, we analyze the effect of several parameters on the gain, computed as described above. Given the amount of control parameters that act on the gain, we decided to focus on the input power, the group velocity mismatch and the injection angle of the pump. In addition to that, we do not consider the effect of birefringence on the filter on the first two cases, but only on the third one. All the parameters of interest are listed in the caption of the figures.

Fig. (2) is a 2D plot of the gain as function of input power P_{IN}. Given the symmetric nature of the gain, we only show the positive tongue of the gain. As expected, the gain increases as the P_{IN} increases, and the most instable frequency tends to shift to the higher values.

Fig. (3) is a 2D plot which shows the dependency of the gain from the group velocity mismatch $\Delta\beta_1$ inside a range of $\pm\,3\;ps\;m^{-1}$. In the plot we can clearly see the signature of GTF, with the gain bands fixed in their position at about $\pm 475\;GHz$ from the pump. In addition to those, we see the typical

gain bands expanding from low to high frequencies, creating a discontinued arch. The discontinuity is due to the presence of the filter, which modify the gain profile. This instability gain plot predicts a very rich dynamic, but in practice the control over the group velocity mismatch is limited.

Fig. (4) depict the evolution of the instability gain as function of the injection angle. In this case we accounted for the effect of the birefringence in the FBG, by assuming two different Bragg frequencies of $\omega_s = -314\ GHz, \omega_f = -322\ GHz$ from the pump.
The main effect of the injection angle is to project the total input power on the two polarization axes as $P_{INx} = P_{IN}|\cos(\chi)|^2$ and $P_{INy} = P_{IN}|\sin(\chi)|^2$. In general, if $\chi \neq \frac{k\,\pi}{2}\ k \in N$, both axes receive a fraction of the total P_{IN}, so the instabilities will grow at the same frequencies on both polarizations. An interesting effect can be observed if we take into account the birefringence in the FBGs. Since the GTF instability band position is related to the Bragg frequency of the filter, different Bragg frequencies will destabilize different bands. Pumping the cavity and filter at different angles of injection, will focus more power on the fast or the slow axes, giving an overall gain on the fast or slow Bragg frequency of the filter. This is what we can see in the plot: as the angle of injection is changed, one of the axes receive more power than the other, allowing the instability gains corresponding to the axes to grows. Is interesting to note how some angles allows two different gain peaks to survive.

Fig. (5) is an example of numerical integration of the LLE, with the signal in time and frequency domain. Red traces are for the x axis, and blue traces are for the y axis. For this simulation we configured the system to have an angle of injection $\chi = 0.88\ rad$, which project more power on the y axis than the x axis. As explained with the previous example, that allows to excite the instability in an asymmetric fashion on the two polarizations axis, which bring to two slightly different spectra. Fig. (6) zoom on the third harmonic components of the spectra of Fig. (5): it's clearly visible the slight difference in the peak position of the two spectra.

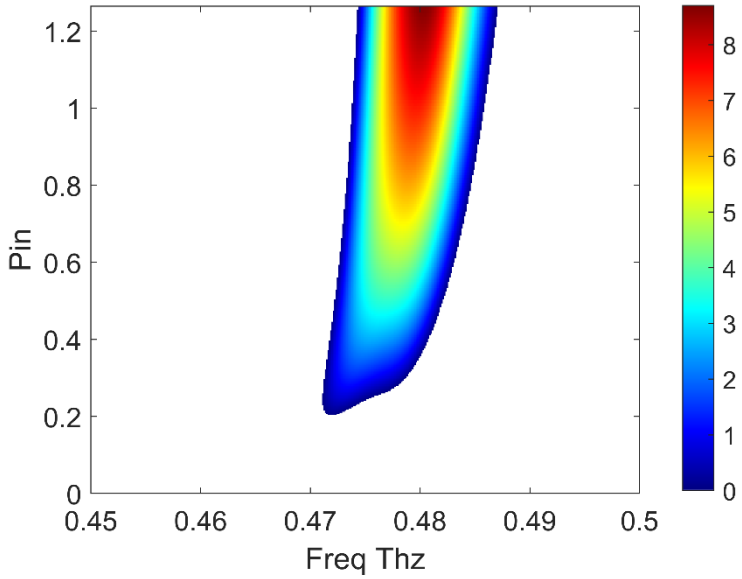

Fig. (2) 2D plot of the evolution of the gain as function of input power P_{IN}. The gain is symmetric, so only the positive tongue is reported. Parameters used are: $\beta_2 = 0.5ps^2km^{-1}, \Delta\beta_1 = 0.5\ ps\ m^{-1}, \chi = \frac{\pi}{4}, \sigma = \frac{2}{3}, \gamma = 2.5W^{-1}km^{-1}, L = 100m, \rho = \sqrt{0.9}\,, \theta = \sqrt{0.1}\,, \phi_{0x,y} = -\psi_{x,y}(0), a = 85\frac{rad}{ns}\ b = -2.45,\ \omega_{f,s} = -314\ GHz.$

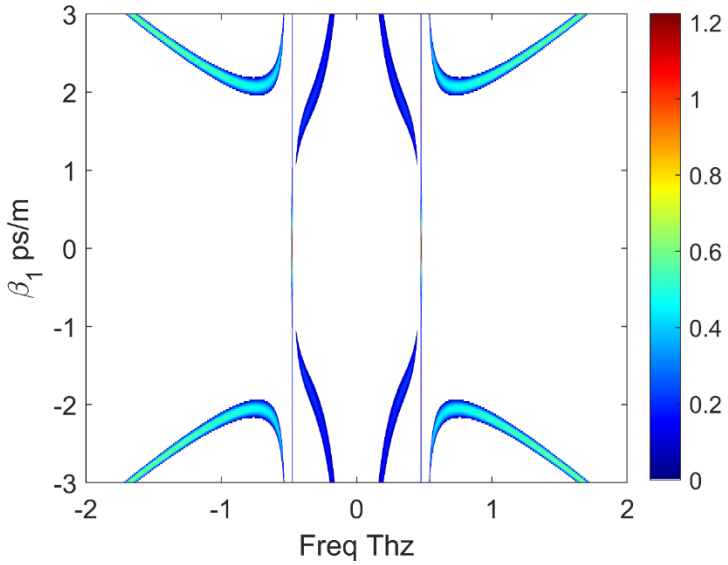

Fig. (3) 2D plot of the evolution of the gain as function of group velocity mismatch $\Delta\beta_1$. Parameters used are: $\beta_2 = 0.5ps^2km^{-1}, \chi = \frac{\pi}{4}, \sigma = \frac{2}{3}, \gamma = 2.5W^{-1}km^{-1}, L = 100m, \rho = \sqrt{0.9}\,, \theta = \sqrt{0.1}\,, \phi_{0x,y} = -\psi_{x,y}(0), a = 85\frac{rad}{ns}\ b = -2.45,\ \omega_{f,s} = -314\ GHz, P_{IN} = 0.5\ W.$

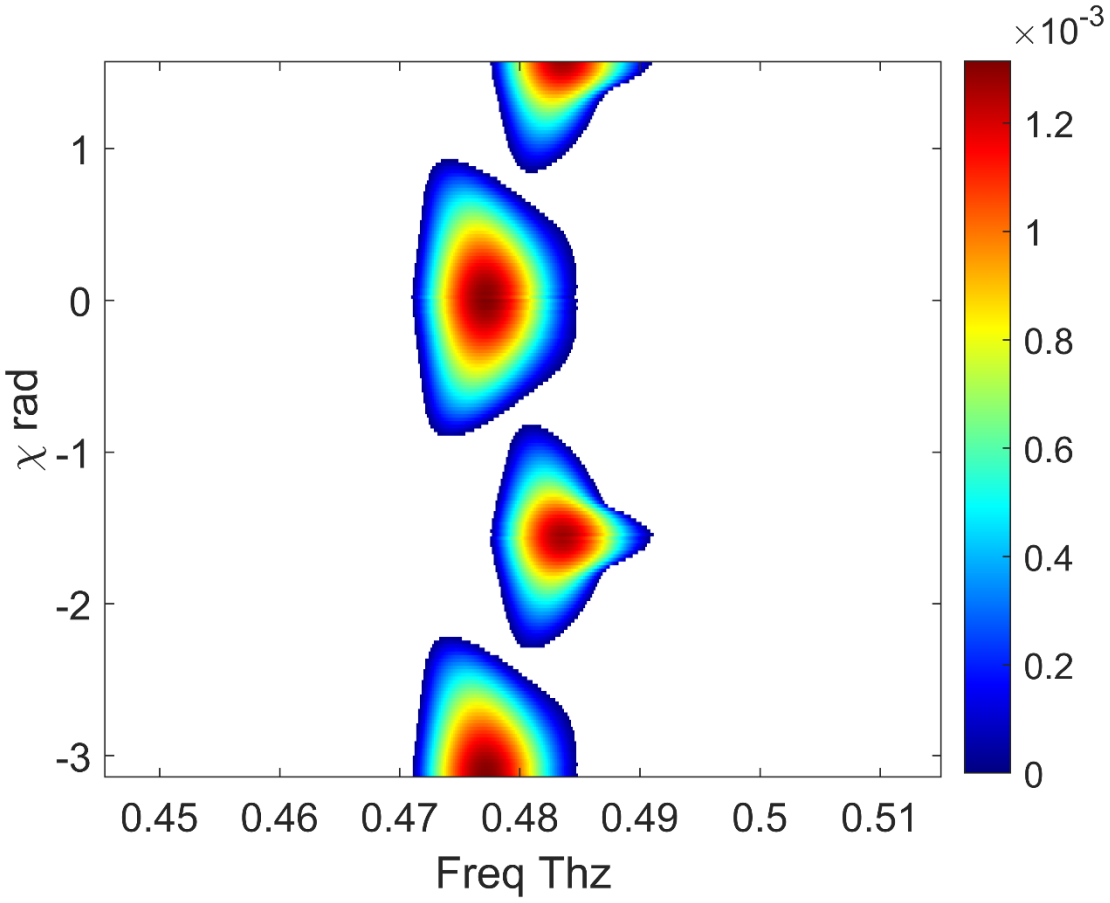

Fig. (4) 2D plot of the evolution of the gain as function of angle of pump injection χ. Parameters used are: $\beta_2 = 0.5ps^2km^{-1}, \sigma = \frac{2}{3}, \gamma = 2.5W^{-1}km^{-1}, L = 100m, \rho = \sqrt{0.9}\,, \theta = \sqrt{0.1}\,, \phi_{0x,y} = -\psi_{x,y}(0), a = 85\frac{rad}{ns}$ $b = -2.45,\ \omega_s = -314\ GHz, \omega_f = -322\ GHz, P_{IN} = 0.5\ W.$

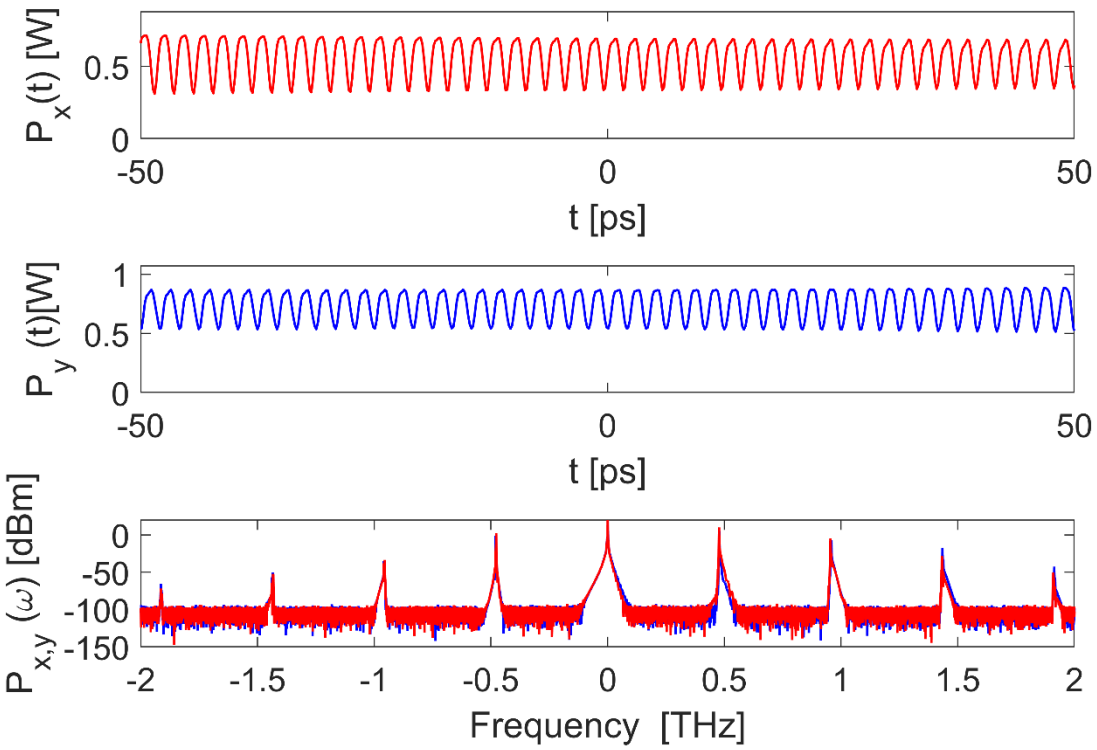

Fig. (5) Example of numerical integration of the LLE model of the PM cavity and filter. The parameter used are: $\beta_2 = 0.5ps^2km^{-1}, \sigma = \frac{2}{3}, \gamma = 2.5W^{-1}km^{-1}, L = 100m, \rho = \sqrt{0.9}\,, \theta = \sqrt{0.1}\,, \phi_{0x,y} = -\psi_{x,y}(0), a = 85\frac{rad}{ns}$ $b = -2.45,\ \omega_s = -314\ GHz, \omega_f = -315\ GHz, P_{IN} = 1\ W.$

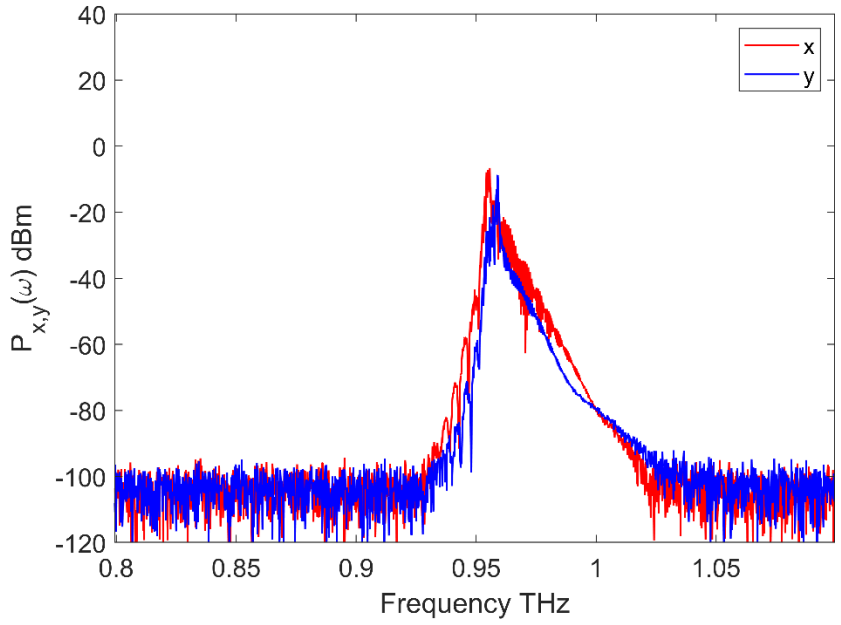

Fig. (6) Zoom on the gird harmonic of the spectra of Fig. (5)

Conclusion:

In this report we proposed an investigation of a PM fibre ring cavity which include a PM FBG. We showed how is it possible to model the problem with a classical LLE approach to give a good representation of filtered induce MI.
We also shown an example of how, by choosing an appropriate set of parameters, the spectra generated on the two axis seems to have a slightly different repetition rate, feature particularly interesting in the double frequency comb framework.

Next steps:

Given those encouraging results, the next step would be an experimental verification of those preliminary findings.

References:

[1]

F. Bessin *et al.*, 'Gain-through-filtering enables tuneable frequency comb generation in passive optical resonators', *Nature Communications*, vol. 10, no. 1, Art. no. 1, Oct. 2019, doi: 10.1038/s41467-019-12375-3.

[2]

A. M. Perego, A. Mussot, and M. Conforti, 'Theory of filter-induced modulation instability in driven passive optical resonators', *Phys. Rev. A*, vol. 103, no. 1, p. 013522, Jan. 2021, doi: 10.1103/PhysRevA.103.013522.

This Project has received funding from the European Union's Horizon 2020 research and innovation programme under the Marie Sklodowska-Curie grant agreement No 861152